Electronic Supplementary Material (ESI) for Journal of Materials Chemistry A.

A Bidirectional Electrocatalyst for Enhancing Li_2S Nucleation and Decomposition Kinetics in Lithium-Sulfur Batteries

Yilun Ren[=], Shaozhong Chang[=], Libing Hu[=], Biao Wang, Dongyue Sun, Hao Wu, Yujie Ma, Yurong Yang, Shaochun Tang, Xiangkang Meng **

National Laboratory of Solid State Microstructures, Collaborative Innovation Center of Advanced Microstructures, College of Engineering and Applied Sciences, Nanjing University, Jiangsu, 210093, China

[*] Corresponding authors:

Email: tangsc@nju.edu.cn; mengxk@nju.edu.cn

[=] These authors contributed equally to this work.

Experimental Section

Figure S1 to Figure S27

Table S1 to Table S3

Experimental Section

Materials: MAX (Ti_3AlC_2) powder was purchased from Jilin 11 Technology Co. Ltd. Hydrochloric acid (HCl), lithium fluoride (LiF), and ethanol were purchased from Nanjing Chemical Reagent Co. Ltd. $CoCl_2 \cdot 6H_2O$ (99.99% AR, grade), $NiCl_2 \cdot 6H_2O$ (99.99%, AR, grade), multiwalled carbon nanotubes (MWCNTs), selenium (Se) and N, N-dimethylformamide (DMF) were obtained from Aladdin Reagent. 1,4-Benzenedicarboxylic acid (1,4-BDC) and triethylamine (TEA) were purchased from Tianjin Fuchen Chemicals Reagent Factory. All chemicals were used directly without further purification. The deionized (DI) water was purified using a Milli-Q3 System (Millipore, France).

Preparation of $Ti_3C_2T_x$/Ni-Co MOF Nanosheets: $Ti_3C_2T_x$/Ni-Co MOFs were prepared by using the method as described in a previous report[1]. First, 100 mg $Ti_3C_2T_x$ was dispersed in a solution containing 32 ml DMF, 2 ml ethanol and 2 ml DI water. Next, 0.375 mmol $NiCl_2 \cdot 6H_2O$, 0.375 mmol $CoCl_2 \cdot 6H_2O$ and 0.75 mmol 1,4-BDC were dissolved into the above solution. Subsequently, 0.8 ml TEA was quickly injected into the mixed solution. The solution was stirred and then continuously ultrasonicated for 8 h under sealed conditions. Finally, $Ti_3C_2T_x$/Ni-Co MOFs were collected after centrifugation, washing and drying at 50 ℃ for 24 h under vacuum conditions. The Ni-Co MOF was prepared in the same way without adding $Ti_3C_2T_x$.

Preparation of Ti_3C_2/$(NiCo)_{0.85}Se$: The Ti_3C_2/$(NiCo)_{0.85}Se$ sample was synthesized via a gas-phase selenization method. Se powder (0.4 g) in a porcelain boat was placed in upstream and 0.2 g $Ti_3C_2T_x$/Ni-Co MOF was placed downstream of a tube furnace. Then, the materials in the porcelain boats were reacted at 500 °C for 2 h with a heating rate of 2 °C min^{-1} under an Ar/H_2 (9:1) atmosphere. Black Ti_3C_2/$(NiCo)_{0.85}Se$ powders were obtained after naturally cooling down under Ar/H_2 flow. Similarly, $(NiCo)_{0.85}Se$ composites were prepared by one-pot selenization by using Ni-Co MOF as precursors.

Materials Characterization: X-ray diffraction (XRD, PANALYTICAL) was used to investigate the crystal structures of the composites from 5° to 80°. The elemental compositions of the surface of the composites were obtained with an ESCALAB250 X-ray photoelectron spectroscopy (XPS, Thermo Fisher Scientific). The structure and morphology of the samples were characterized by transmission electron microscopy (TEM, JEM-2100F) and the scanning electron microscopy (SEM, Hitachi S-4800). The elemental mappings of the samples were recorded by energy-dispersive spectroscopy (EDS). Thermogravimetric analysis (TGA, NETZSCH-Gertebau GmbH, Germany) was used to confirm the contents of each section of the samples in nitrogen flow with a heating rate of 10 °C min^{-1} from 50 °C to 800 °C. Raman spectra were determined with a Renishaw inVia spectrometer system with a 532 nm laser. The specific surface of the samples was measured by the Brunauer–Emmett–Teller method (kubo X1000, China). UV–Vis spectroscopy measurements were collected from a SHIMADZU UV-3600 spectrometer.

Visualized Adsorption of Lithium Polysulfides: A 20 mM Li_2S_6 solution was prepared by dissolving Li_2S (purity>99.9%, Aladdin) and S (molar ratio of 1:5) into 1,2-dimethoxyethane (DME) and 1,3-dioxolane (DOL), followed by vigorous stirring at 50 °C for 24 h. Typically, 20 mg of the samples was added to 1.0 mL Li_2S_6 solution.

Nucleation Tests of Li_2S: 0.5 M Li_2S_8 solution was homemade by stirring Li_2S and S (molar ratio of 1:7) in tetraethylene glycol solvent for 24 h. Ti_3C_2/$(NiCo)_{0.85}Se$, Ti_3C_2 and $(NiCo)_{0.85}Se$ were dispersed in ethanol, dropped onto carbon paper (CP) disks with a diameter of 12 mm and dried at 50 °C for 24 h. The modified CP disks with a loading of 1 mg cm^{-2}, lithium foil and Celgard 2500 membrane were used as the cathode, anode and separator to assemble coin cells, respectively. Then, 20 μL of 1.0 M LiTFSI electrolyte was added to the anode side, and 20 μL Li_2S_8 solution was added to the cathode side. The cell was galvanostatically discharged to 2.06 V at 0.112 mA, and then discharged potentiostatically at 2.02 V for 20000 seconds. The precipitation capacity of Li_2S can be calculated through Faraday's Law.

Dissolution Tests of Li_2S: Except for the catalyst electrode, the cells for the Li_2S dissolution tests were identical to those in the measurement of Li_2S nucleation. The cells were first galvanostatically discharged to 1.7 V at 0.10 mA and then discharged galvanostatically to 1.7 V at 0.01 mA for fully converting LiPS to solid Li_2S. Finally, the cells were charged potentiostatically at 2.35 V until 30000 s for the sufficient dissolution of Li_2S.

***Assembly of Li_2S_6 Symmetric Cells*:** Symmetric cells were assembled with two identical electrodes of Ti_3C_2/$(NiCo)_{0.85}Se$, Ti_3C_2 and $(NiCo)_{0.85}Se$ loaded onto CP disks. 0.2 M Li_2S_6 solution (in DME/DOL) solution containing 1.0 M LiTFSI and 0.5 M $LiNO_3$ was used as the electrolyte. Cyclic voltammetry (CV) tests were carried out at scan rates from 0.5 to 10 mV s^{-1} between -0.8 V and 0.8 V on a CHI660D electrochemical workstation. The symmetric cell with Ti_3C_2/$(NiCo)_{0.85}Se$ electrodes without Li_2S_6 was assembled and tested as a control experiment.

Preparation of Ti_3C_2/$(NiCo)_{0.85}Se$@PP Separators: The modified commercial polypropylene celgard (PP) separator was obtained by a typical doctor-blade coating method. The as-synthesized Ti_3C_2/$(NiCo)_{0.85}Se$, MWCNTs and PVDF with a weight ratio of 8:1:1 using NMP as the solvent were mixed, and then coated onto PP. The obtained Ti_3C_2/$(NiCo)_{0.85}Se$@PP separator was dried under vacuum at 50 °C for 24 h and cut into 16 mm circular disks for direct use. The Ti_3C_2@PP or $(NiCo)_{0.85}Se$@PP separator was prepared through similar procedures except Ti_3C_2/$(NiCo)_{0.85}Se$ was replaced by Ti_3C_2 or $(NiCo)_{0.85}Se$.

Preparation of HPGC/S: The $HPGC^2$/S composites were prepared using a conventional melt-diffusion method. In a typical procedure, HPGC and S were mixed with an appropriate mass ratio of 8:2 and then heated at 155 °C for 16 h. The product was collected after cooling to room temperature to generate the HPGC/S composite.

Electrochemical Tests: A homogeneous slurry was prepared by mixing HPGC/S, polyvinylidene fluoride (PVDF, 5%) and acetylene black in a weight ratio of 7:2:1, and then the slurry was cast on Al foil and dried at 60 °C for 24 h in a vacuum oven to obtain the electrode film. Subsequently, the disks with a diameter of 10 mm were obtained by cutting the electrode film, and the loading of active materials on each disk was approximately 1.5 mg cm^{-2} (N/P ratio is 16.7). And for the high loading test, the sulfur loading is 6.4 mg cm^{-2} (N/P ratio is 3.9). The electrochemical tests were carried out by using CR2032-type coin cells that were assembled in an Ar-filled glove box. The anode, separator, and electrolyte were commercial Li metal (15.6 mm in diameter), modified Celgard 2500 and the solution by adding 1 M lithium bis(trifluoromethanesulfonyl) imide (LiTFSI) and 0.5 M $LiNO_3$ in DOL/DME (1:1 by volume) solvents, respectively. The electrolyte/sulfur (E/S) was maintained at ~20 μL mg^{-1} per cell. CV tests were carried out at scan rates of 0.1 mV s^{-1} between 1.7 V and 2.8 V on a CHI660D electrochemical workstation, and electrochemical impedance spectroscopy (EIS) was performed using an Autolab electrochemical workstation over a frequency range of 0.01 Hz-10 kHz. The galvanostatic charge-discharge profiles were obtained using a Land battery tester with a voltage from 1.7 to 2.8 V *vs* Li^+/Li.

Calculations for Diffusion Coefficient of Li Ions: The coefficient of Li^+ diffusion can be estimated by the Randles-Sevcik equation:

$$I_p = (2.69 * 10^5)\, n^{3/2} S D^{1/2} C v^{1/2}$$

where I_p is the peak current, n is the transferred electrons number, S is the area of the electrode, D is the Li^+ diffusion coefficient, C is the concentration change of Li^+ during the electrochemical reaction, and v is the CV scan rate. The n, S, and C are constant, thus, I_p and $v^{1/2}$ have a linear relationship, and D is positively correlated with the slopes of the curves (I_p - $v^{1/2}$).

Computational Methods: We employed the Vienna Ab Simulation Initio Package (VASP)[3, 4] to perform all density functional theory (DFT) calculations within the generalized gradient approximation (GGA) using the PBE[5] formulation. We have

chosen the projected augmented wave (PAW) potentials[6, 7] to describe the ionic cores and take valence electrons into account using a plane wave basis set with a kinetic energy cut-off of 400 eV. Partial occupancies of the Kohn−Sham orbitals were allowed using the Gaussian smearing method and a width of 0.03 eV. The electronic energy was considered self-consistent when the energy change was smaller than 10^{-4} eV. During structural optimizations, the Brillouin zone was sampled by 3×3×2 k-points (Monkhorst–Pack) in $(NiCo)_{0.85}Se$ and a 1×1×1 Monkhorst-Pack k-point grid in $Ti_3C_2/(NiCo)_{0.85}Se$. The binding strength Eb of lithium polysulfides on the $(NiCo)_{0.85}Se$ and $Ti_3C_2/(NiCo)_{0.85}Se$ surfaces was calculated as follows: $E_b = (E_{sub} + E_{lp}) - E_{sub+lp}$, where E_{sub+lp}, E_{lp}, and E_{sub} denote the calculated energies of the total adsorption system, adsorbates, and substrates, respectively. The free energy was calculated using the equation: G=E+ZPE-TS, where G, E, ZPE and TS are the free energy, total energy from DFT calculations, zero-point energy and entropic contributions, respectively. Finally, the free energies (G) of different intermediates are defined as $\Delta G=G_i-G_r$ (G_i is the energy of intermediates and G_r is the total energy of reactants). The kinetic barriers of Li_2S dissociation were located using the climbing-image nudged elastic band (CINEB) method[8].

Supplementary Figures and Tables

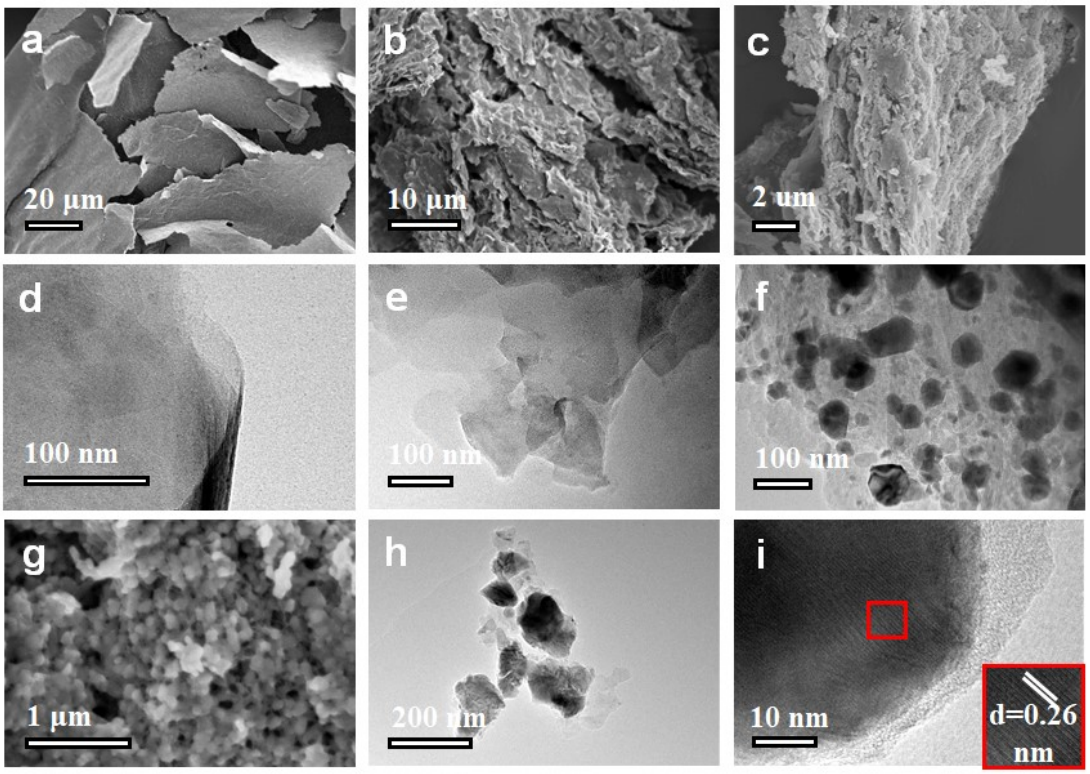

Figure S1. a) SEM and d) TEM images of $Ti_3C_2T_x$; b) SEM and e) TEM images of $Ti_3C_2T_x$/Ni-Co MOF; c) SEM and f) TEM images of Ti_3C_2/$(NiCo)_{0.85}Se$; g) SEM and h) TEM images of $(NiCo)_{0.85}Se$; i) HRTEM images of $(NiCo)_{0.85}Se$.

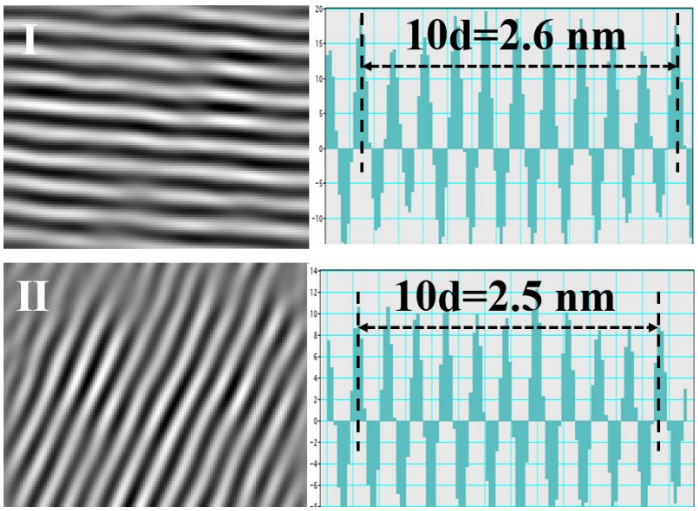

Figure S2. Fourier transformed crystalline lattice, corresponding to the HRTEM image.

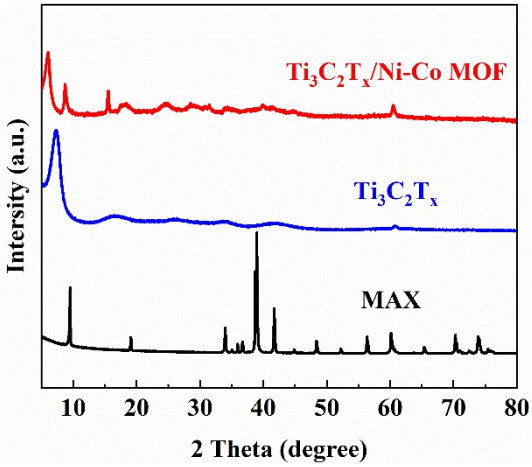

Figure S3. XRD pattern of Ti_3C_2/Ni-Co MOF, $Ti_3C_2T_x$ and MAX.

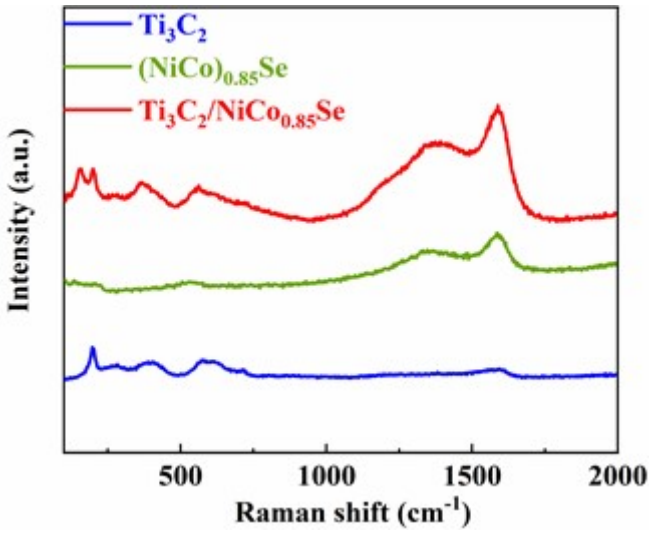

Figure S4. Raman spectra of $Ti_3C_2/(NiCo)_{0.85}Se$, Ti_3C_2 and $(NiCo)_{0.85}Se$.

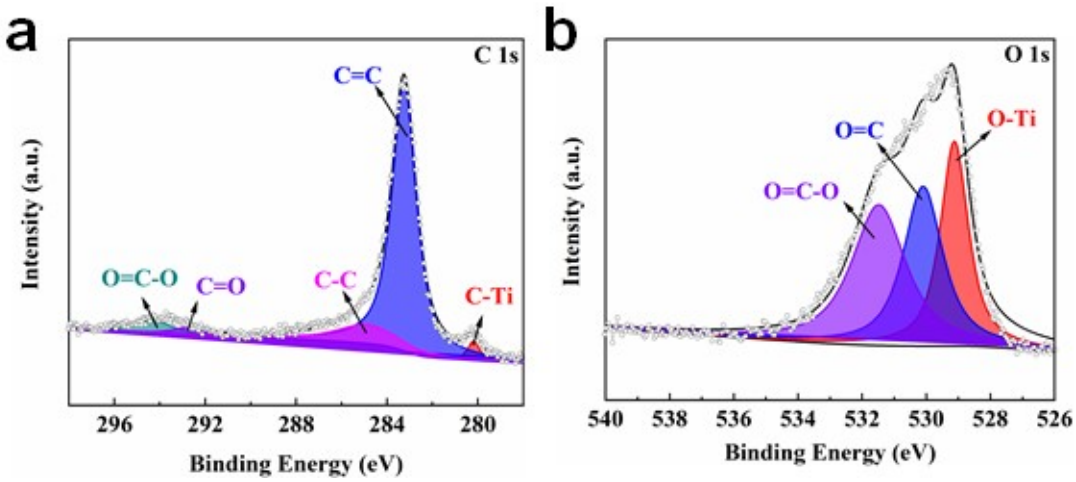

Figure S5. High-resolution a) C 1s and b) O 1s XPS spectra of $Ti_3C_2/(NiCo)_{0.85}Se$.

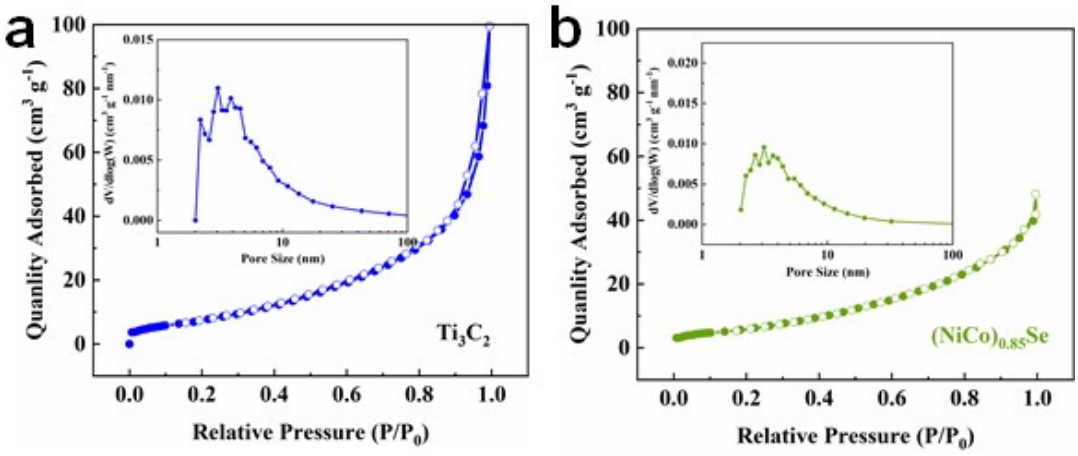

Figure S6. N_2 adsorption–desorption isotherm curves and the pore size distribution of a) Ti_3C_2 and b) $(NiCo)_{0.85}Se$.

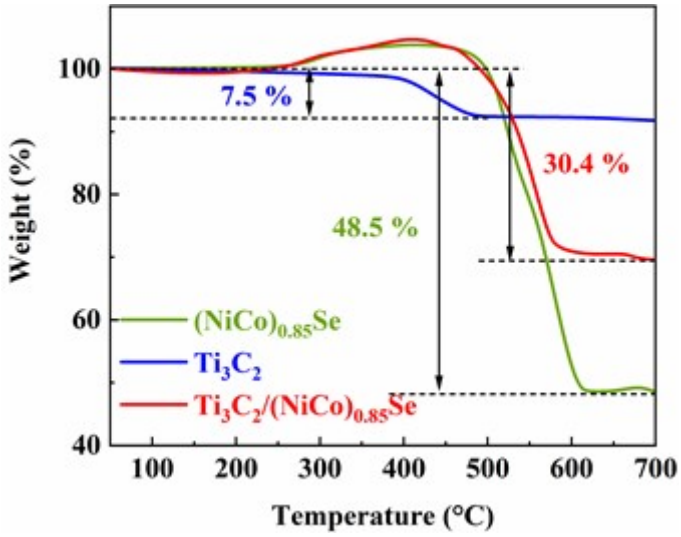

Figure S7. TGA of $Ti_3C_2/(NiCo)_{0.85}Se$, Ti_3C_2 and $(NiCo)_{0.85}Se$.

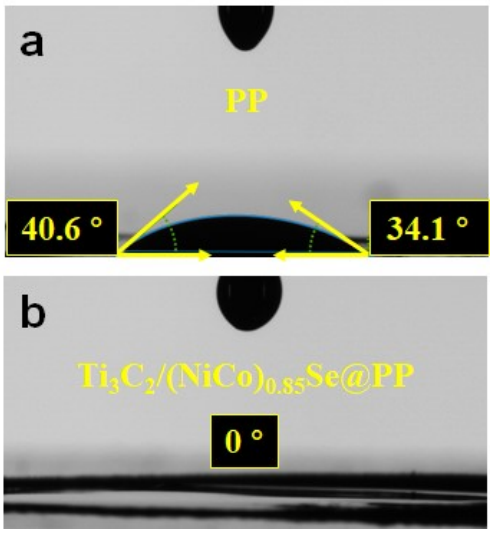

Figure S8. The electrolyte contact angle shots of the a) PP and b) $Ti_3C_2/(NiCo)_{0.85}Se$@PP.

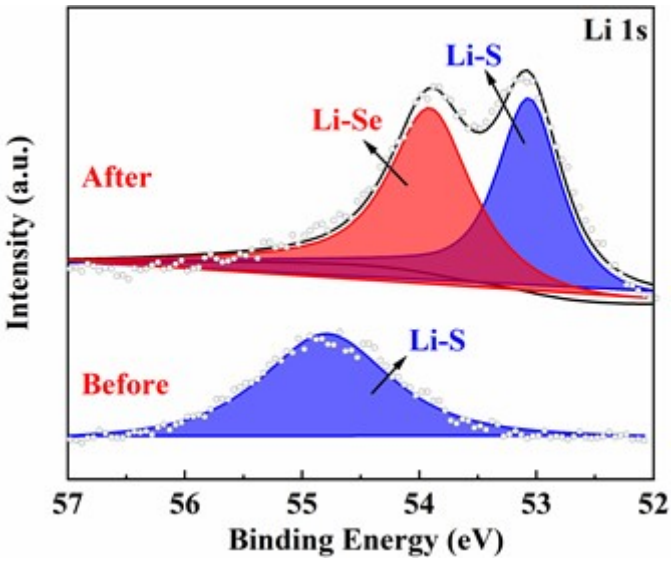

Figure S9. High-resolution Li 1s XPS spectra of Li_2S_6 before and after adsorption.

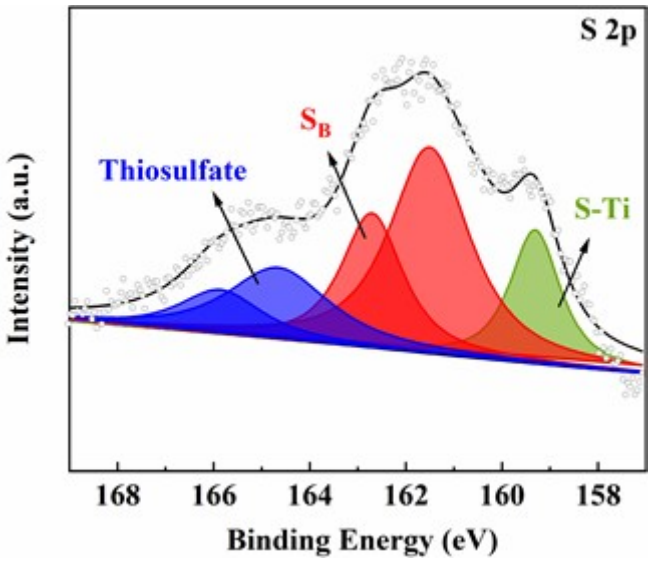

Figure S10. High-resolution S 2p XPS spectra of Li_2S_6 after adsorption.

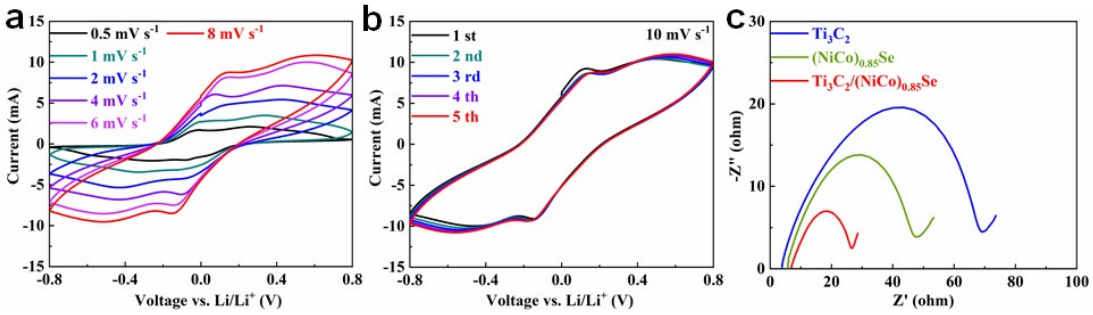

Figure S11. CV profiles at a) different scanning rates (0.5-8 mV S^{-1}) and b) 10 mV s^{-1} of $Ti_3C_2/(NiCo)_{0.85}Se$ symmetrical cells. c) EIS curves of symmetric cells.

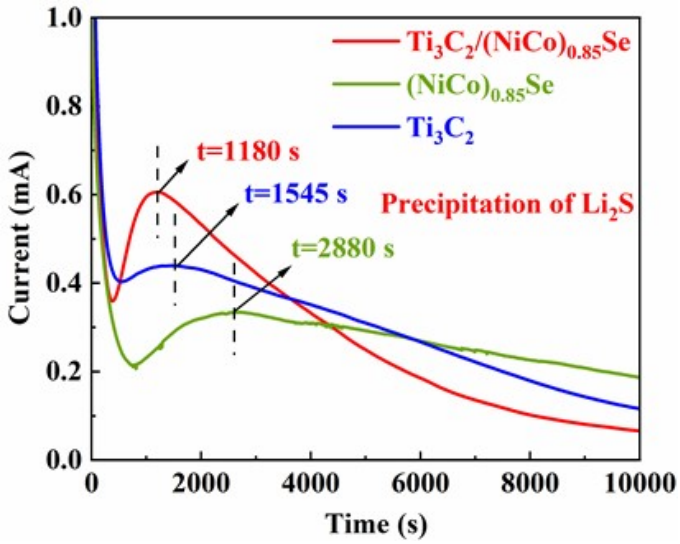

Figure S12. Potentiostatic discharge curves of $Ti_3C_2/(NiCo)_{0.85}Se$, Ti_3C_2 and $(NiCo)_{0.85}Se$.

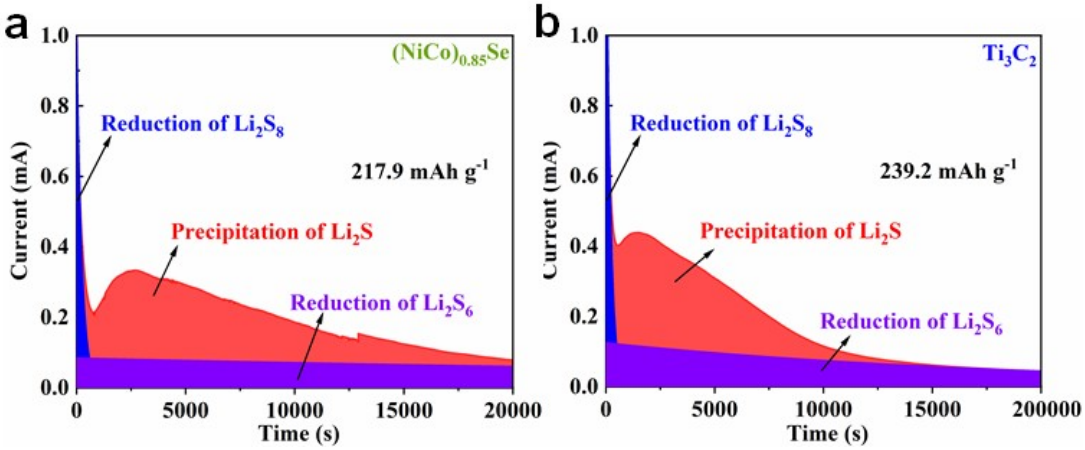

Figure S13. Potentiostatic discharge fitted curves of $(NiCo)_{0.85}Se$ and Ti_3C_2.

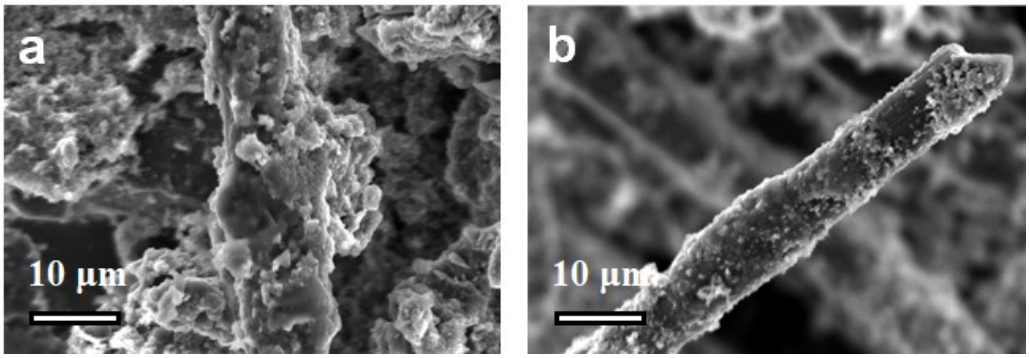

Figure S14. SEM images of the precipitation of Li_2S on a) Ti_3C_2 and b) $(NiCo)_{0.85}Se$ electrodes.

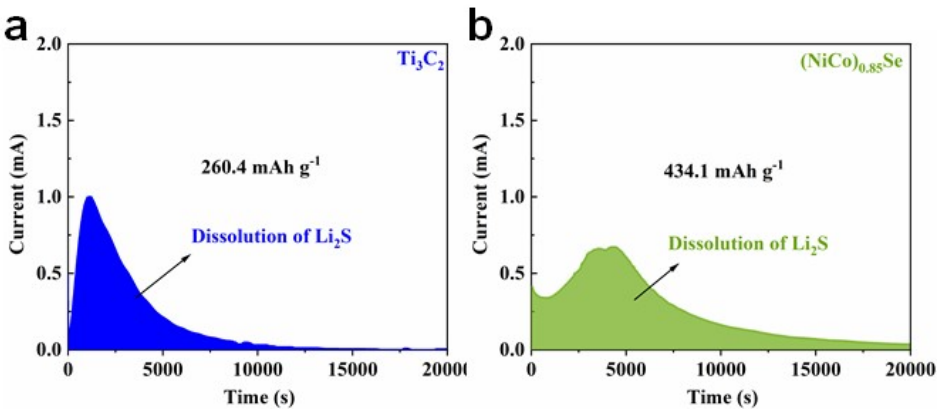

Figure S15. Potentiostatic charge fitted curves of a) Ti_3C_2 and b) $(NiCo)_{0.85}Se$.

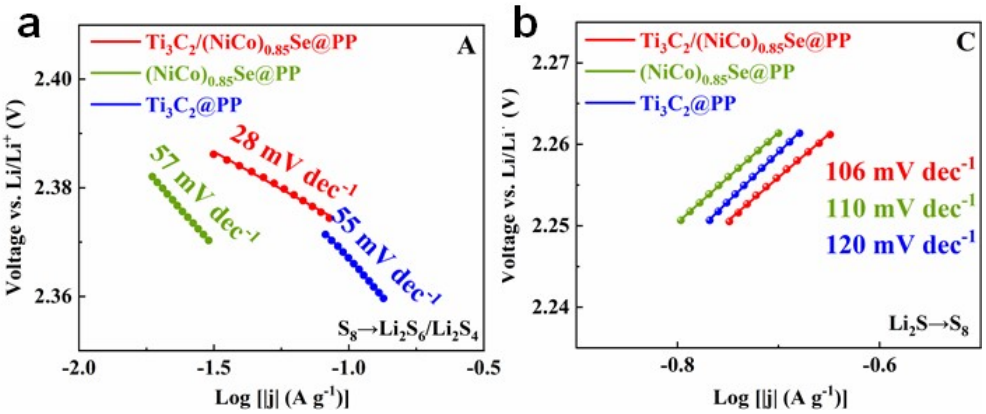

Figure S16. The Tafel plots calculated from the a) A and b) C peaks of Ti_3C_2@PP, $(NiCo)_{0.85}Se$@PP and $Ti_3C_2/(NiCo)_{0.85}Se$@PP.

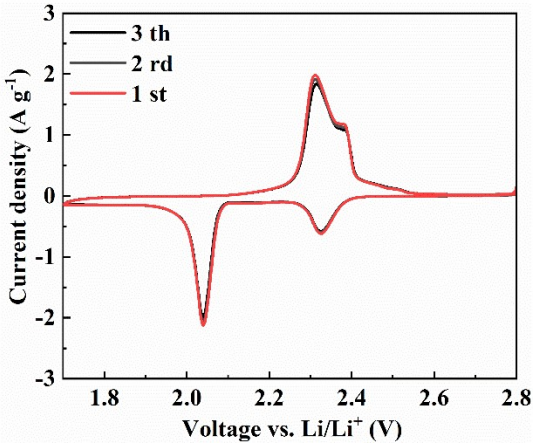

Figure S17. CV curves of the $Ti_3C_2/(NiCo)_{0.85}Se$@PP cell.

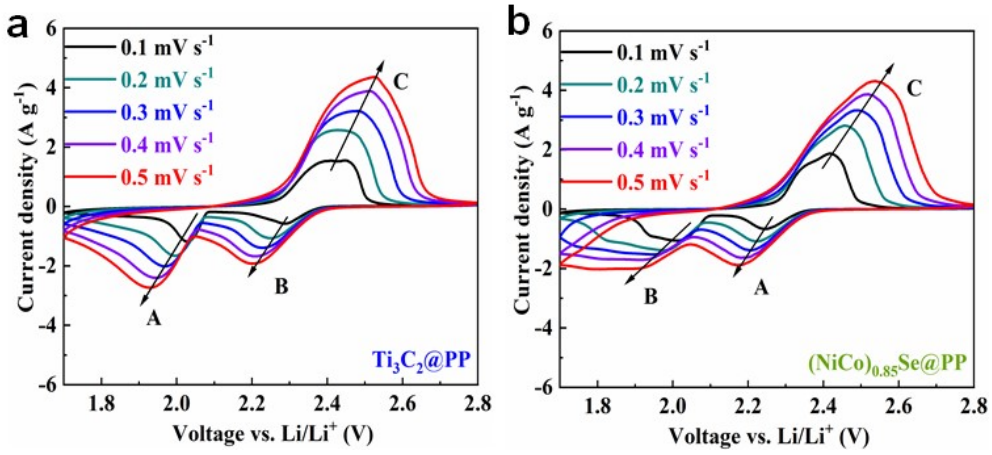

Figure S18. CV curves of a) Ti_3C_2@PP and b) $(NiCo)_{0.85}Se$@PP cells.

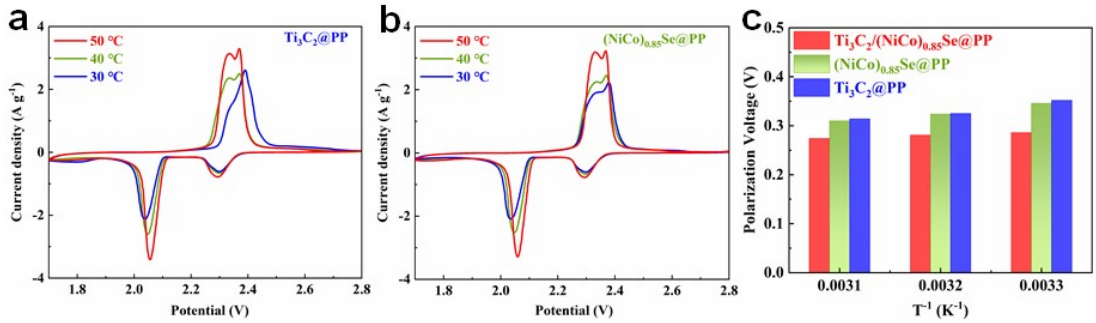

Figure S19. CV curves of a) Ti_3C_2@PP and b) $(NiCo)_{0.85}Se$@PP cells at various temperatures. c) Polarization voltage gaps of cathodic peaks C and anodic peaks A.

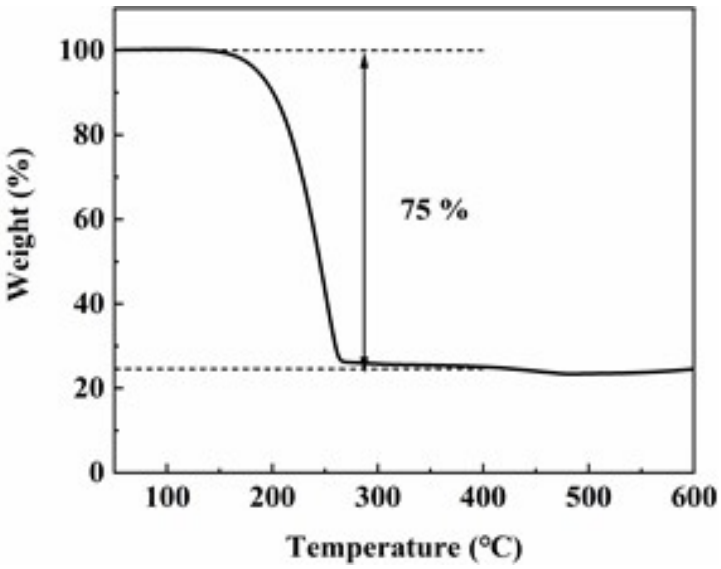

Figure S20. TGA curves of HPGC/S.

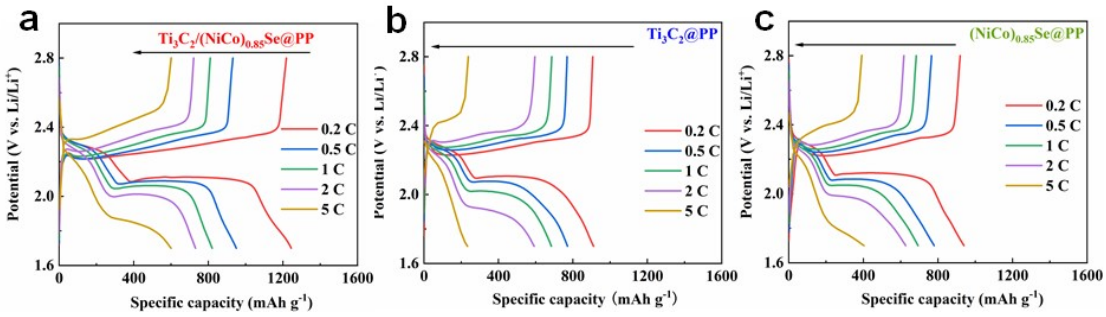

Figure S21. Charge–discharge profiles of the a) Ti_3C_2/$(NiCo)_{0.85}Se$@PP, b) Ti_3C_2@PP and c) $(NiCo)_{0.85}Se$@PP separators.

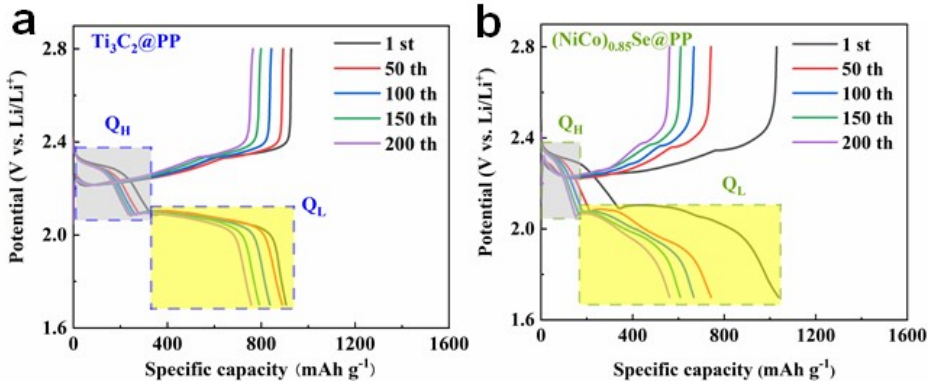

Figure S22. Galvanostatic charge–discharge profiles of the Ti_3C_2@PP and $(NiCo)_{0.85}Se$@PP separators with different numbers of cycles at 0.2 C.

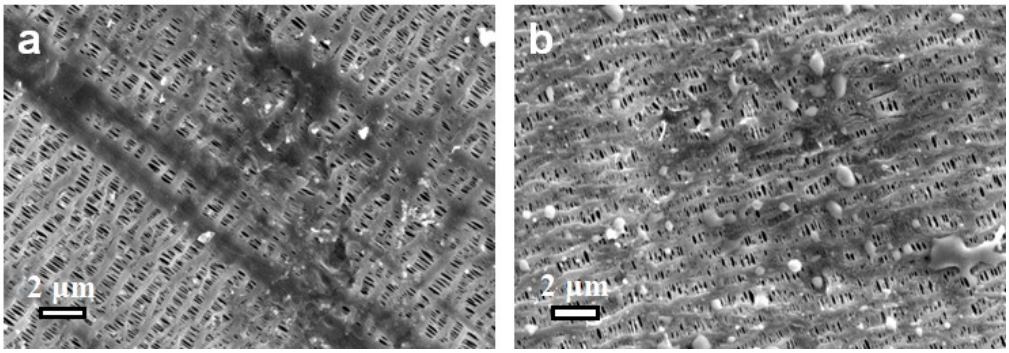

Figure S23. SEM images for (a) Ti_3C_2@PP and (b) $(NiCo)_{0.85}Se$@PP toward the lithium anode after 200 cycles at 0.2 C.

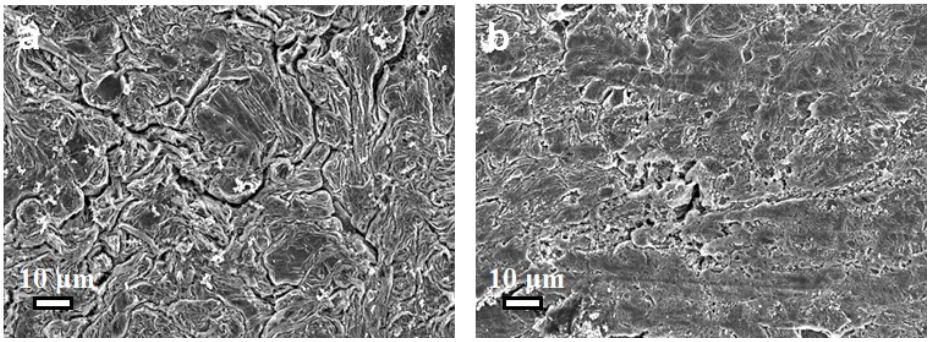

Figure S24. SEM images of lithium metal anodes after 200 cycles at 0.2 C for (a) Ti_3C_2@PP and (b) $(NiCo)_{0.85}Se$@PP.

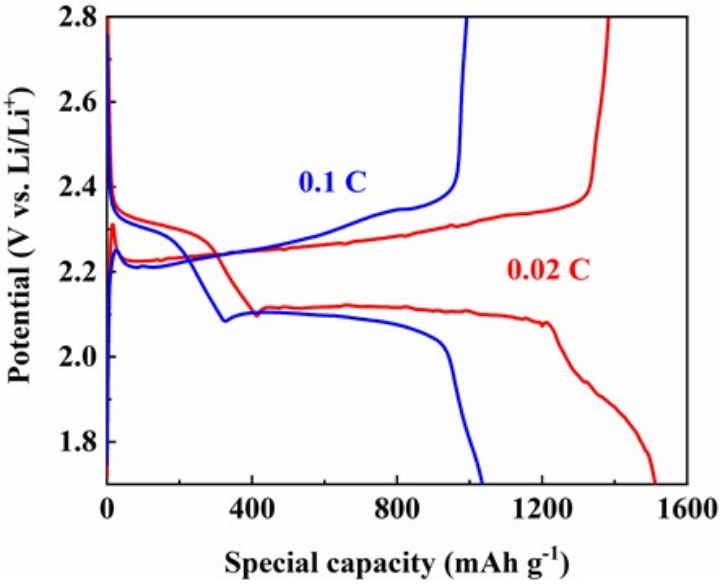

Figure S25. Charge–discharge profiles of $Ti_3C_2/(NiCo)_{0.85}Se$@PP.

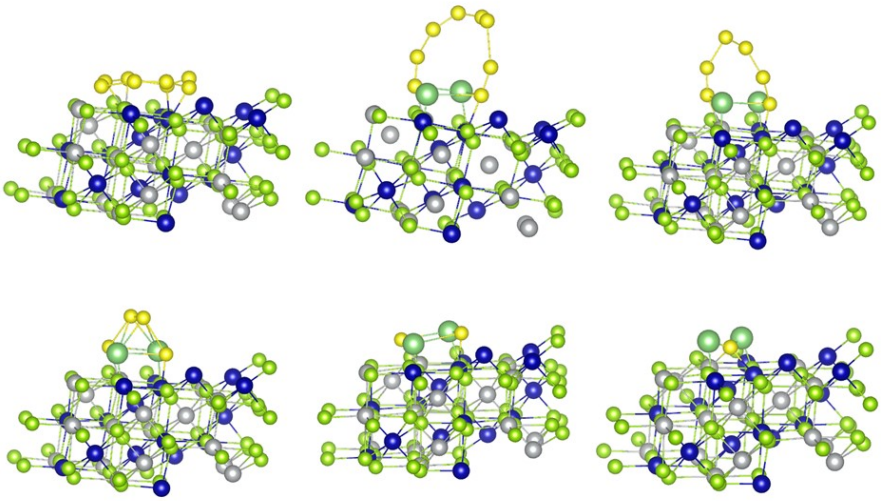

Figure S26. The optimized adsorption structures of sulfur species on the $(NiCo)_{0.85}Se$ substrate.

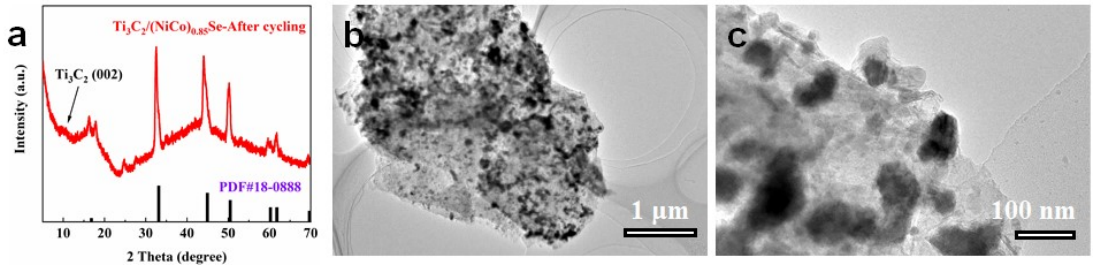

Figure S27. a) XRD pattern and b-c) TEM images of $Ti_3C_2/(NiCo)_{0.85}Se$ after 100 cycles at 1 C.

Table S1 BET surface area and total pore volume of Ti_3C_2/$(NiCo)_{0.85}Se$, $(NiCo)_{0.85}Se$ and Ti_3C_2.

Sample	BET surface area (m^2 g^{-1})	Total pore volume (cm^3 g^{-1})
Ti_3C_2/$(NiCo)_{0.85}Se$	**91.839**	**0.138**
$(NiCo)_{0.85}Se$	**46.736**	**0.062**
Ti_3C_2	**56.218**	**0.112**

Table S2. EIS results of Ti_3C_2/$(NiCo)_{0.85}Se$@PP, $(NiCo)_{0.85}Se$@PP and Ti_3C_2@PP before cycling.

Seperator	Rs (Ω)	Rct (Ω)
$Ti_3C_2T_x$/Ni-Co MOF@PP	1.6	16.6
$Ti_3C_2T_x$@PP	1.9	31.2
PP	2.2	29.1

Table S3. Comparison of electrochemical performance of our work with various works.

	Sulfur content (wt %)	Sulfur loading (mg cm^{-2})	Current density (C)	Cycle number	Capacity decay per cycle (%)
This work	**80**	**1.5**	**1**	**2000**	**0.03**
Co-Bi/rGO[9]	70	1.1	1	500	0.051
S/V-N-C[10]	75	1.5	1	1000	0.056
$CoSe_2$/hNCTs/S[11]	80	1.3	1	1000	0.069
CoZn-S[12]	70	1	1	1800	0.04
S@Co–Fe–P[13]	71	1	1	500	0.043
P-$Mo_{0.9}Co_{0.1}S_2$-2[14]	80	2	1	600	0.046
FPGS[15]	80	1	0.5	500	0.05
CoNiP/rGO/S[16]	60	1.5	1	600	0.08
S@CoNi MOF[17]	86.5	1.5	1	500	0.036

References

1. Ren, Y.; Zhai, Q.; Wang, B.; Hu, L.; Ma, Y.; Dai, Y.; Tang, S.; Meng, X. Synergistic Adsorption-Electrocatalysis of 2D/2D heterostructure toward high performance Li-S batteries. *Chem. Eng. J.* 2022, 439, 135535.
2. Hu, Q.; Lu, J.; Yang, C.; Zhang, C.; Hu, J.; Chang, S.; Dong, H.; Wu, C.; Hong, Y.; Zhang, L. Promoting Reversible Redox Kinetics by Separator Architectures Based on CoS_2/HPGC Interlayer as Efficient Polysulfide-Trapping Shield for Li-S Batteries. *Small* 2020, 16, 2002046.
3. Kresse, G.; Furthmuller, J. Efficiency of ab-initio total energy calculations for metals and semiconductors using a plane-wave basis set. *Comput. Mater. Sci.* 1996, 6, 15-50.
4. Kresse, G.; Furthmuller, J. Efficient iterative schemes for ab initio total-energy calculations using a plane-wave basis set. *Phys. Rev. B* 1996, 54, 11169-11186.
5. Perdew, J. P.; Burke, K.; Ernzerhof, M. Generalized gradient approximation made simple (vol 77, pg 3865, 1996). *Phys. Rev. Lett.* 1997, 78, 1396-1396.
6. Blochl, P. E. Projector augmented-wave method. *Phys. Rev. B Condens. Matter.* 1994, 50, 17953-17979.
7. Kresse, G.; Joubert, D. From ultrasoft pseudopotentials to the projector augmented-wave method. *Phys. Rev. B* 1999, 59, 1758-1775.
8. Yu, M.; Trinkle, D. R. Accurate and efficient algorithm for Bader charge integration. *J. Chem. Phys.* 2011, 134, 064111.
9. Li, C.; Qi, S.; Zhu, L.; Zhao, Y.; Huang, R.; He, Y.; Ge, W.; Liu, X.; Zhao, M.; Xu, L.; Qian, Y. Regulating polysulfide intermediates by ultrathin Co-Bi nanosheet electrocatalyst in lithium−sulfur batteries. *Nano Today* 2021, 40, 101246.
10. Yu, S.; Sun, Y.; Song, L.; Cao, X.; Chen, L.; An, X.; Liu, X.; Cai, W.; Yao, T.; Song, Y.; Zhang, W. Vanadium atom modulated electrocatalyst for accelerated Li-S chemistry. *Nano Energy* 2021, 89, 106414.
11. Su, H.; Lu, L.; Yang, M.; Cai, F.; Liu, W.; Li, M.; Hu, X.; Ren, M.; Zhang, X.; Zhou, Z. Decorating $CoSe_2$ on N-doped carbon nanotubes as catalysts and efficient polysulfides traps for Li-S batteries. *Chem. Eng. J.* 2022, 429, 132167.
12. Ye, Z.; Jiang, Y.; Li, L.; Wu, F.; Chen, R. Synergetic Anion Vacancies and Dense Heterointerfaces into Bimetal Chalcogenide Nanosheet Arrays for Boosting Electrocatalysis Sulfur Conversion. *Adv. Mater.* 2022, e2109552.
13. Chen, Y.; Zhang, W.; Zhou, D.; Tian, H.; Su, D.; Wang, C.; Stockdale, D.; Kang, F.; Li, B.; Wang, G. Co-Fe Mixed Metal Phosphide Nanocubes with Highly Interconnected-Pore Architecture as an Efficient Polysulfide Mediator for Lithium-Sulfur Batteries. *ACS Nano* 2019, 13, 4731-4741.
14. Lin, H.; Zhang, S.; Zhang, T.; Ye, H.; Yao, Q.; Zheng, G. W.; Lee, J. Y. Simultaneous Cobalt and Phosphorous Doping of MoS_2 for Improved Catalytic Performance on Polysulfide Conversion in Lithium–Sulfur Batteries. *Adv. Energy Mater.* 2019, 9, 1902096.
15. Zhang, Y.; Wang, Y.; Luo, R.; Yang, Y.; Lu, Y.; Guo, Y.; Liu, X.; Cao, S.; Kim, J. K.; Luo, Y. A 3D porous FeP/rGO modulated separator as a dual-function polysulfide barrier for high-performance lithium sulfur batteries. *Nanoscale Horiz.* 2020, 5, 530-540.
16. Xiao, T.; Yi, F.; Yang, M.; Liu, W.; Li, M.; Ren, M.; Zhang, X.; Zhou, Z. A composite of CoNiP quantum dot-decorated reduced graphene oxide as a sulfur host for Li–S batteries. *J. Mater. Chem. A* 2021, 9, 16692-16698.

17. Meng, R.; Du, Q.; Zhong, N.; Zhou, X.; Liu, S.; Yin, S.; Liang, X. A Tandem Electrocatalysis of Sulfur Reduction by Bimetal 2D MOFs. *Adv. Energy Mater.* 2021, 11, 2102819.